Hindawi Publishing Corporation
Journal of Nanomaterials
Volume 2016, Article ID 8095737, 9 pages
http://dx.doi.org/10.1155/2016/8095737

Research Article

Highly Efficient Adsorption of Aqueous Pb(II) with Mesoporous Metal-Organic Framework-5: An Equilibrium and Kinetic Study

José María Rivera,[1] Susana Rincón,[2] Cherif Ben Youssef,[3] and Alejandro Zepeda[4]

[1]*Facultad de Ciencias Químicas, Universidad Veracruzana, Prolongación Oriente 6, No. 1009 Colonia Rafael Alvarado, 94340 Orizaba, VER, Mexico*
[2]*Instituto Tecnológico de Mérida, Av. Tecnológico km 4.5, 97118 Mérida, YUC, Mexico*
[3]*Instituto Tecnológico de Cancún, DEPI, Av. Kabah km 3, 77500 Cancún, QROO, Mexico*
[4]*Facultad de Ingeniería Química, Universidad Autónoma de Yucatán, Campus de Ingenierías y Ciencias Exactas, Periférico Norte km 33.5, 97203 Mérida, YUC, Mexico*

Correspondence should be addressed to Alejandro Zepeda; zepeda74@yahoo.com

Received 18 August 2016; Accepted 4 October 2016

Academic Editor: Shu Seki

Mesoporous metal-organic framework-5 (MOF-5), with the composition $Zn_4O(BDC)_3$, showed a high capacity for the adsorptive removal of Pb(II) from 100% aqueous media. After the adsorption process, changes in both morphology and composition were detected using a scanning electron microscope (SEM) equipped with an energy dispersive X-ray (EDX) system, Fourier transform infrared spectroscopy (FTIR), and X-ray photoelectron spectroscopy (XPS) analysis. The experimental evidence showed that Zn(II) liberation from MOF-5 structure was provoked by the water effect demonstrating that Pb(II) removal is not due to ionic exchange with Zn. A kinetic study showed that Pb(II) removal was carried out in 30 min with a behavior of pseudo-second-order kinetic model. The experimental data on Pb(II) adsorption were adequately fit by both the Langmuir and BET isotherm models with maximum adsorption capacities of 658.5 and 412.7 mg/g, respectively, at pH 5 and 45°C. The results of this work demonstrate that the use of MOF-5 has great potential for applications in environmental protection, especially regarding the removal of the lead present in industrial wastewaters and tap waters.

1. Introduction

As a result of intensive industrial activity, wastewaters have been increasingly contaminated by heavy metals capable of causing severe health and environmental problems. These undesired wastes are principally formed in the industrial production of fertilizers, batteries, paints, ceramics, glass, explosives, and photography products, as well as metal-extractive industries [1, 2]. Once heavy metals are introduced into living organisms (including humans), they tend to accumulate and promote a variety of physiological disorders [1]. Lead, in particular, is one of the most disturbing metals in the environment and is considered highly dangerous in terms of environmental risk. Exposure to lead can cause mental deficiency, convulsions, and reduction in hemoglobin production, which may cause anemia [3, 4]. To prevent environmental exposure, the US Environmental Protection Agency [5] has established a maximum concentration of Pb(II) in drinking water of 0.015 mg/L. As a consequence, industrial effluents containing high lead concentrations must be treated before being discharged into water bodies.

Different techniques are used to eliminate Pb(II) from wastewaters, including chemical precipitation, membrane filtration, ion-exchange resins, solvent extraction, adsorption, and coprecipitation [6–8]. However, the applications of these methods in some cases are costly with disadvantages such as incomplete removal and the generation of toxic wastes that require further treatment [7]. Adsorption, in particular, has shown promising results in water treatment in terms of easy operation, high removal efficiency, and its applicability for various pollutants. So far, different materials for removal

of Pb(II) of water and wastewater by adsorption have been reported, such as dry desulfurization slag [9], magnetic modified sugarcane bagasse [10], hydroxyapatite [11], biochar-alginate capsule [12], and chitosan/Fe-hydroxyapatite nanocomposite [13]. The porous materials are generally considered as efficient adsorbents for organic compounds and heavy metals [14–16].

Recently, a new class of mesoporous materials called metal-organic frameworks (MOFs) have attracted considerable attention as they combine properties of both organic and inorganic materials [15, 16]. Various studies using MOFs as adsorbent material for gas and organic compound removal have shown good adsorption capacities [17–24]. However, only few studies have used MOFs as adsorbent material for heavy metal adsorption in aqueous media, and there is therefore scarce information about the possible interaction mechanisms between the adsorbent and the adsorbate. In particular, Bakhtiari and Azizian [25] have recently presented evidence of Cu^{2+} adsorption in aqueous media with MOF-5 (consists of Zn_4O inorganic moiety that acts as secondary building unit, coordinating to benzene 1,4-dicarboxylate, a bidentate ligand that acts as spacers, to form a three-dimensional structure). The authors suggested that the obtained 290 mg/g of Cu^{2+} maximum adsorption capacity may be explained by the heterogenic surface of MOF-5 which contains different active sites for adsorption. However, they did not reveal sufficient information to explain the possible mechanisms of adsorption or interactions between adsorbent and adsorbate, as well as the effect of water (at 100%) on the morphology and structure of MOF-5 when it is known that, from 4% of water, MOF-5 may present changes in the crystalline morphology, superficial area, and pore size [21, 26].

In this context, we found it necessary to further investigate the constitutive bonding interactions as well as the structural stability in aqueous media of the MOFs, in particular MOF-5. The main objective of this study was to better understand the behavior of MOF-5 during the adsorption process in aqueous media. For this purpose, MOF-5 was synthesized, characterized, and used as adsorbent material for the removal of Pb(II) from aqueous media (100%). The adsorption kinetics, pH influence, isotherms, and surface chemistry were investigated.

2. Material and Methods

2.1. Reagents. All reactants and solvents were purchased from the Aldrich Chemical Co. MOF-5 was synthesized in a glass reactor equipped with reflux condenser and Teflon-lined stirrer; 2 g of terephthalic acid and 9.31 g of zinc nitrate hexahydrate were dissolved in 60 mL of *N,N′*-dimethylformamide (DMF) solution and heated up to 150°C for 4 h. After that, the product was cooled down to room temperature. The Pb(II) solutions were obtained by dilution from a stock solution containing 1000 mg Pb(II)/L to obtain metal concentrations from 30 to 200 mg/L. Aqueous solutions containing 0.1 M HCl and 0.1 M NaOH were used to determine the removal capacity of Pb(II) at different pH values.

2.2. Characterizations. The size, morphology, and chemical composition of MOF-5 before and after the adsorption process were analyzed using a scanning electron microscope (SEM). The SEM was equipped with an energy dispersive X-ray (EDX) system (Phillips XL30 model). Fourier transform infrared spectroscopy (FTIR) was achieved by the Thermo Nicolet Nexus 670 FT-IR spectrometer using KBr pellets. X-ray photoelectron spectroscopy (XPS) was achieved by the Thermo Scientific K-alpha spectrometer. Powder X-Ray Diffraction (XRD) patterns were obtained in a Bruker D8-Advance instruments with 40 kV, 30 mA for $Cu_{K\alpha}$ (λ = 1.5416 Å) radiation, with a scan speed of 1°/min and a step size of 0.02° in 2θ.

2.3. Adsorptive Removal of Pb(II) from Aqueous Media. MOF-5 (0.025 g) was weighed into an Erlenmeyer flask. Solutions (100 mL) of Pb(II) with concentrations ranging from 30 to 100 mg/L were used at initial pH at 5, without addition of NaOH or HCl, with a stirring velocity at 200 rpm for 6 h. All of the studies were carried out at 27, 35, and 45°C. After 6 h, centrifugation (15000 rpm during 20 min) was used to separate the MOF-5 from the solution, and filtration was performed using a nylon membrane with a 0.22 μm pore size. The obtained solution was used for the measurement of Pb(II) concentration. To monitor the adsorption kinetics, samples were taken at various time intervals from an Erlenmeyer flask with an initial concentration of 200 mg Pb(II)/L, reacted at a pH of 5 and a stirring rate of 200 rpm for 6 h. To evaluate the possible liberation of Zn(II) due to aqueous conditions (100%), an additional set of experiments was performed under the same previous experimental conditions but without addition of Pb(II). The Pb(II) and Zn(II) concentrations were measured by flame atomic absorption using a Perkin Elmer AA800 spectrometer. All experiments were conducted at least in triplicate.

The adsorption capacity at equilibrium q_e (in mg/g) was calculated using the following relation:

$$q_e = \frac{(C_0 - C_e) \times V}{W}, \quad (1)$$

where C_0 is the initial concentration of Pb(II) (mg/L), C_e is the equilibrium concentration of Pb(II) (mg/L), V is the volume of the aqueous solution (L), and W is the weight of MOF-5 (g).

3. Results and Discussion

3.1. Characterization of MOF-5 before and after the Pb(II) Adsorption Process

3.1.1. SEM and EDX Characterization. The morphology of MOF-5 and its chemical composition were determined before and after the Pb(II) adsorption process using a SEM (Figure 1) equipped with an EDX (Figure 3) and XRD (Figures 1S and 2). The images obtained by SEM before Pb(II) removal (Figure 1(a)) show not well defined structure of MOF-5. Additionally Figure 2(a) shows the disappearance of the peak at 6.9° and the decrease of intensity of peak at 9.7°. This

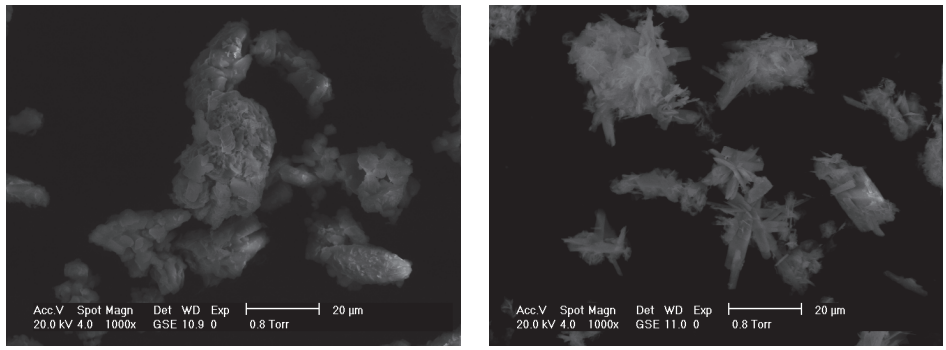

(a) (b)

Figure 1: SEM images of MOF-5; (a) before Pb(II) adsorption; (b) after Pb(II) adsorption.

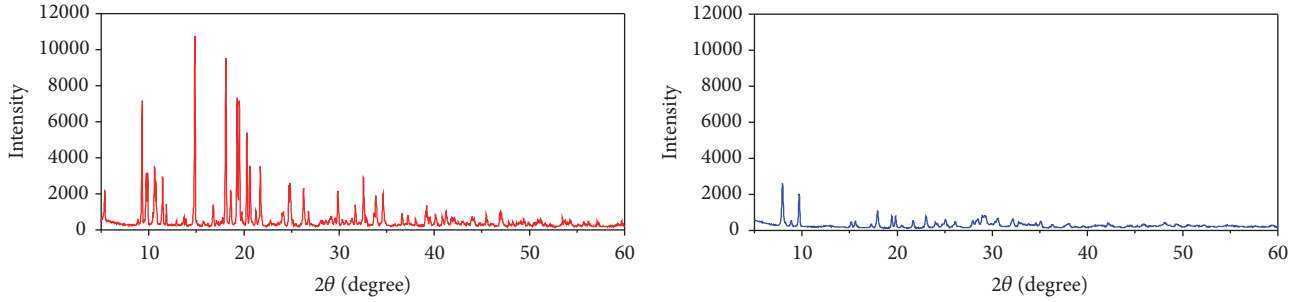

(a) (b)

Figure 2: XRD pattern of MOF-5; (a) before Pb(II) adsorption; (b) after Pb(II) adsorption.

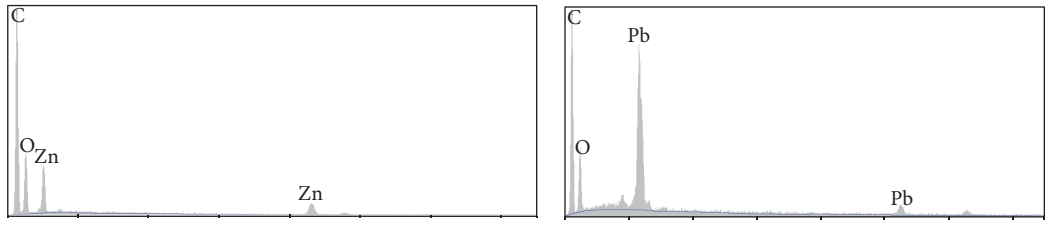

(a) (b)

Figure 3: EDX spectra of MOF-5; (a) before Pb(II) adsorption; (b) after Pb(II) adsorption.

occurrence may be due to humidity adsorption (presence of water) as reported by Rodríguez et al. [26]. However the XRD pattern obtained after the synthesis of MOF-5 (Figure 1S) shows the MOF-5 characteristic peaks at 6.9° and 9.7° corresponding to a trigonal symmetry as reported in [30]. After Pb(II) removal, a significant change in the MOF-5 morphology took place resulting in a complex twinning rod-shaped material (Figure 1(b)). Moreover, significant changes occurred in the XRD pattern, where the disappearance of peak at 6.9° and a low intensity of peak at 9.7° (Figure 2(b)) were observed. These changes may be explained by the effect of the aqueous medium on MOF-5. Greathouse and Allendorf [31] observed that at low water content the MOF-5 structure is maintained and that at higher water contents, 3.9% and 9.5%, the MOF-5 structure collapsed. This instability may lead to changes in pore size, material structure, surface area, and material diffusion [26, 32–36].

The results of EDX analysis before and after Pb(II) removal (Figures 3(a) and 3(b)) showed that after the adsorption process, the entirety of the 9.78% mass component of Zn(II) is missing, while Pb(II) amounting to 32.86% by mass has been adsorbed by the MOF-5 (Table 1). In order to better explain the liberation of Zn(II) shown by the EDX analysis, complementary experiments were realized according to the methodology previously described (100 mL volume, pH 5.6, and 0.025 g MOF-5) in the absence and presence of Pb(II). It was observed that the liberated Zn(II) was 63.7 ± 1.7 mg Zn(II)/L in both cases. These results indicate that Pb(II)

Table 1: EDX composition of MOF-5 before and after the removal of Pb(II).

MOF-5 before removal of Pb(II)			MOF-5 after removal of Pb(II)		
Element	Mass (%)	Atom (%)	Element	Mass (%)	Atom (%)
C	68.21	78.77	C	53.18	81.11
O	22.01	19.08	O	13.96	15.98
Zn	9.78	2.15	Zn	0	0
Pb	0	0	Pb	32.86	2.91

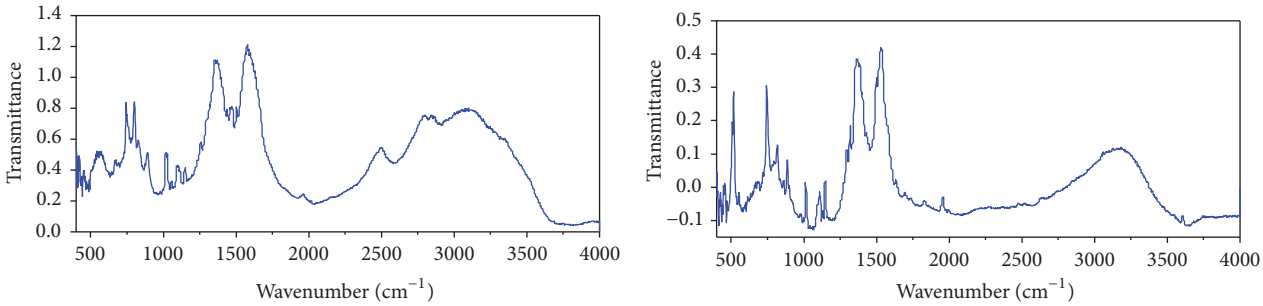

Figure 4: FTIR spectra of MOF-5; (a) before Pb(II) adsorption; (b) after Pb(II) adsorption.

incorporation and the liberation of Zn(II) result from an adsorption process on the MOF-5 surfaces and that no ionic exchange took place, as has been the case in other reported studies [37]. The loss of Zn(II) in the MOF-5 structure may be due to the coordination of the Zn(II) contained in the Zn_4O complexes with the oxygen atoms of the water through unbonded (electrostatic and van der Waals) interactions [31], provoking the liberation of benzene dicarboxylate ion (BDC^{2-}) which directly interacts with Pb(II).

3.1.2. FTIR Characterization. The infrared spectra of MOF-5 samples before and after the Pb(II) adsorption process are presented in Figure 4. For the sample of adsorbent material before the adsorption process, the characteristic MOF-5 signals observed at 1587 and 1359 cm^{-1} (Figure 4(a)) correspond to the asymmetric and symmetric stretching of the C-O bond of the carboxylate group directly bonded to Zn, respectively [38, 39]. It is observed that for the sample extracted at the end of the adsorption process (Figure 4(b)), the signal at 1587 cm^{-1} shifted to 1530 cm^{-1}. This change may be explained by the absence of Zn and by the union of the C-O bond of the carboxylate group to Pb, which is in accordance with the results of the EDX analysis. It has to be noticed that little absorption is observed for the coordination compounds in the 1800 to 2200 cm^{-1} range where only vibrations of C-O elongation are visible [40]. A characteristic signal of a CO metallic group is observed at 1955 cm^{-1} for both samples. Furthermore, the small bands observed in the 950 to 1225 cm^{-1} range (Figures 4(a)-4(b)) correspond to the flexion of the plane of the C-H group present in the benzene ring of the BDC linker. The bands observed at 806 and 763 cm^{-1} are due to the flexion outside the plane of the C-H group present in the benzene ring of the BDC linker, and only differences in the intensity of the signals before and after Pb(II) adsorption are observed [41]. The wide bands observed at 3090 and 3161 cm^{-1} (Figures 4(a)-4(b)) correspond to the O-H group of the water and indicate the presence of humidity that is frequently located in the metal coordination [42].

3.1.3. XPS Characterization. The XPS pattern of MOF-5 samples before (Figure 5(a)) and after (Figure 5(b)) the Pb(II) adsorption process shows peaks at 284.4 and 284.27 eV for C 1s and at 532.04 and 531.09 eV for O 1s, respectively. The XPS pattern of Zn 2p in MOF-5 is deconvolved into two peaks with binding energies assigned to Zn $2p_{3/2}$ at 1022–1021.98 eV and to Zn $2p_{1/2}$ at 1045.58–1045.19 eV. This is an indication of the presence of the BDC linker coordination which corresponds to the framework groups of the zinc carboxylate [43, 44]. Additionally, a significant decrease of the peaks intensity was observed after Pb(II) adsorption (Figure 5(b)), confirming the liberation of Zn(II). Furthermore, the signal located at 138.25 eV and corresponding to Pb 4f indicates the presence of lead in the adsorbent material, as reported in the formation of PbO [45, 46].

Based on the evidence obtained by Greathouse and Allendorf [31], we propose in this study a possible mechanism for Pb(II) adsorption on MOF-5 in aqueous media. The water molecules that are penetrating the MOF-5 pores provoke interactions between Zn ions and the oxygen atoms of the water through unbonded (electrostatic and Van der Waals) interactions due to the fact that substituents in tetrahedral complexes (Zn_4O) are usually very labile. This phenomenon provokes in turn the formation of BDC^{2-}, which in direct interaction with Pb(II) participates in the formation of

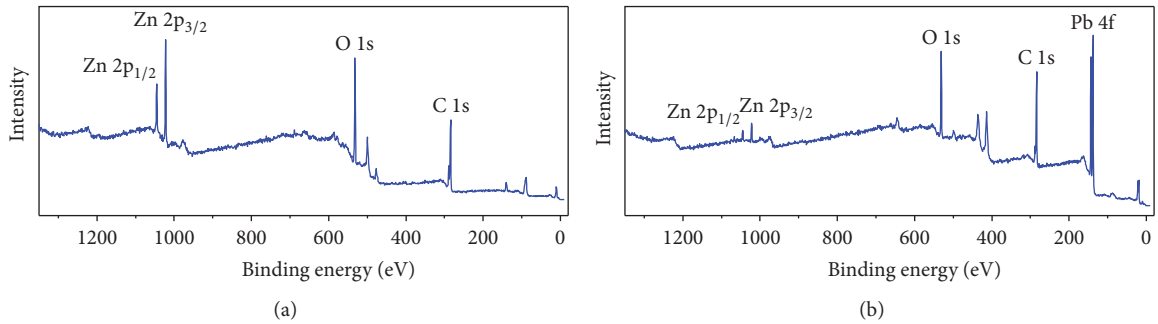

FIGURE 5: XPS spectra of MOF-5; (a) before Pb(II) adsorption; (b) after Pb(II) adsorption.

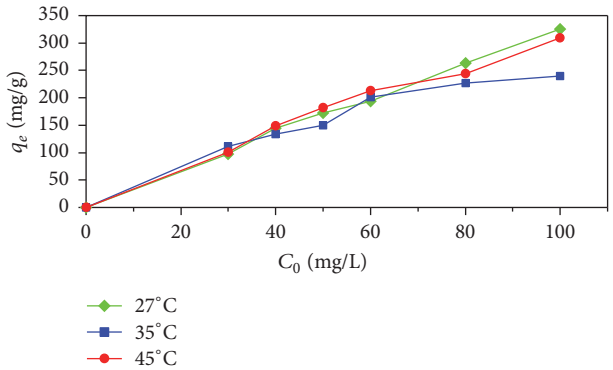

FIGURE 6: Temperature effect on the Pb(II) adsorption capacity (q_e) onto MOF-5 at different initial Pb(II) concentrations (C_0) at pH 5 and 6 h of contact time.

PbBDC structures according to the possible mechanism (ignoring associated hydrolysis reactions):

$$\begin{aligned}&(Zn_4O)(BDC)_3 + 4H_2O\\ &\quad\longrightarrow [(Zn_4O)(H_2O)_4(BDC)_2]^{2+} + BDC^{2-}\\ &[(Zn_4O)(H_2O)_4(BDC)_2]^{2+} + BDC^{2-} + Pb^{2+}\\ &\quad\longrightarrow [(Zn_4O)(H_2O)_4(BDC)_2]^{2+} + PbBDC\end{aligned} \quad (2)$$

3.2. Effect of Temperature (27, 35, and 45°C) on Pb(II) Removal. To study the removal mechanism, superficial properties, and the affinity of MOF-5 for Pb(II), studies were carried out at 27, 35, and 45°C for 6 h at pH 5 using a range of initial Pb(II) concentrations (30, 40, 50, 60, 80, and 100 mg/L). The evolution of the adsorption capacity (q_e) versus the initial concentration of Pb(II) (Figure 6) exhibited a directly proportional relationship, reaching maximum values of 325, 239, and 309 mg/g at 27, 35, and 45°C, respectively.

3.3. Adsorption Isotherms. In this study, equilibrium data were analyzed with the Langmuir and BET adsorption isotherm models at 27, 35, and 45°C. The Langmuir model describes a single-layer adsorption process [47]. The following equations correspond to the nonlinear form (Equation (3)) and the linearized form (4) of the Langmuir isotherm model [48]:

$$q_e = \frac{q_{\max} K_L C_e}{1 + K_L C_e}, \quad (3)$$

$$\frac{C_e}{q_e} = \frac{1}{q_{\max}} \times C_e + \frac{1}{q_{\max} K_L}. \quad (4)$$

In these equations, $q_{\max}$ is the maximum adsorbent capacity (mg/g) and K_L is the Langmuir adsorption constant (L/mg). The constants of the Langmuir model ($q_{\max}$ and K_L) can be evaluated either by nonlinear fitting from (3) or by calculating the slope and the intercept of the linear fitting plot (4), which describes (C_e/q_e) as a function of C_e.

The BET model, which is an extension of the Langmuir model, assumes a multilayer adsorption process. The following equations correspond to the nonlinear (5) and linearized form (Equation (6)) of the BET isotherm model [49]:

$$q_e = \frac{q_{\max} K_B C_e}{(C_s - C_e)\left[1 + (K_B - 1)\, C_e/C_s\right]}, \quad (5)$$

$$\frac{C_e}{(C_s - C_e)\, q_e} = \frac{K_B - 1}{K_B q_{\max}} \times \frac{C_e}{C_s} + \frac{1}{K_B q_{\max}}. \quad (6)$$

In these equations, K_B is the BET adsorption constant (L/mg) and C_s the saturation concentration of Pb(II) (mg/L). Both nonlinear and linearized forms of the Langmuir ((3)-(4)) and BET ((5)-(6)) isotherms for Pb(II) adsorption at 27°C are plotted in Figures 7(a) and 7(b), respectively. Both models could be well fit to the experimental data. Standard nonlinear and linear fitting algorithms (Figure 7) were used to estimate the model parameters, $q_{\max}$ and K_L, for the Langmuir model, and $q_{\max}$ and K_B, for the BET model (Table 2). Good fitting results were obtained for both Langmuir and BET models, although the BET model predicted lower values for the maximal capacity of Pb(II) adsorption at 35°C. The Langmuir value was 234.7 mg/g, whereas the BET value was 162.3 mg/g.

The maximal capacity of Pb(II) adsorption on MOF-5 was estimated to be 658.5 mg/g (at 45°C) using the Langmuir model with the assumption that adsorption occurs in a specific homogeneous place (single layer). This value is higher than those obtained by other studies with different materials. For example, Wu et al. [9] obtained a $q_{\max}$ value of 130.2 mg/g,

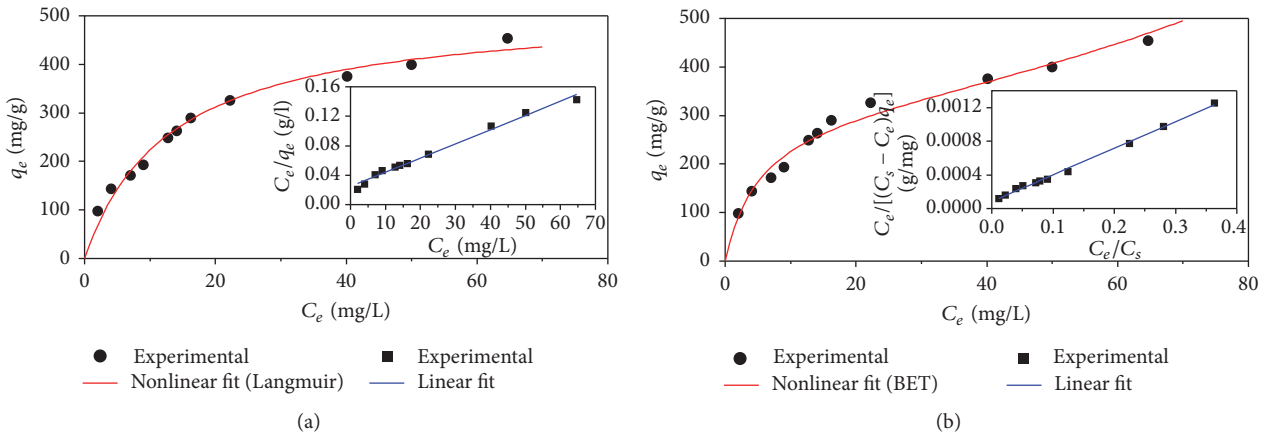

Figure 7: Adsorption isotherms for Pb(II) adsorption over MOF-5 at 27°C and pH 5. Nonlinear and linear fitting for the Langmuir model (a) and the BET model (b).

Table 2: Langmuir and BET isotherm constants for the adsorption of Pb(II) with MOF-5 using nonlinear form (upper value) and linearized form (lower value).

T (°C)	Langmuir model				BET model			
	Equation	q_{max} (mg/g)	K_L (L/mg)	R^2	Equation	q_{max} (mg/g)	K_B (L/mg)	R^2
27	(3)	517.6	0.076	0.98	(5)	323.2	68.5	0.98
	(4)	517.4	0.078	0.98	(6)	315.9	38.3	0.99
35	(3)	234.7	0.518	0.81	(5)	162.3	353.1	0.91
	(4)	256.1	0.330	0.99	(6)	156.5	1390.3	0.99
45	(3)	658.5	0.046	0.98	(5)	412.7	15.6	0.99
	(4)	657.6	0.047	0.94	(6)	418.4	7.6	0.97

which corresponds to only 20% of the capacity obtained in this work (Table 3). These high Pb(II) removal capacities obtained in aqueous media with MOF-5 may be explained by the interaction between the BDC^{2-} and Pb(II), as reported by Greathouse and Allendorf [31].

3.4. Adsorptive Removal Kinetics. A kinetic study of Pb(II) removal with MOF-5 was carried out with an initial concentration of 200 mg/L, a pH of 5, and at 27°C with contact times ranging from 0 to 6 h (Figure 8(a)). The results showed that maximum Pb(II) removal occurs during the first 30 min, reaching 55 ± 1% of the total Pb(II) removal, which may be explained by the high availability of BCD^{-2}. After this initial period, the amount of adsorbed Pb(II) nearly stops as equilibrium is attained.

A pseudo-second-order kinetic model [50] was used to analyze the Pb(II) removal kinetics (Figure 8(b)). Its nonlinear form is given by the following equation:

$$q_t = \frac{k_2 q_e^2 t}{1 + k_2 q_e t}. \quad (7)$$

Its most common linearized form is given by

$$\frac{t}{q_t} = \frac{1}{k_2 q_e^2} + \frac{1}{q_e} t. \quad (8)$$

Here, q_e (mg/g) is the sorption capacity at equilibrium, q_t (mg/g) is the sorption capacity at time t (h), and k_2 is the rate constant. The initial rate of adsorption (h) (mg/g min) can also be calculated by using the following relation [51]:

$$h = k_2 q_e^2. \quad (9)$$

As shown in Figure 8(b), adequate agreement between the model and experimental data was obtained using both the standard nonlinear and linear fitting procedures. High correlation coefficients (0.99) were obtained. The predicted values of q_e are also are close to those found experimentally, suggesting that the adsorption of Pb(II) onto MOF-5 follows pseudo-second-order kinetics. The initial adsorption rate (h), as calculated using (9), was 17% higher (19.88 mg/g min) than the values reported by Sheela and Nayaka [51] for Pb(II) adsorption with NiO nanoparticles (16.45 mg/g min). This difference may be attributed to increased active sites (BDC^{2-}) where Pb(II) may coordinate to be adsorbed.

3.5. Effect of pH on Pb(II) Removal. The removal of Pb(II) from aqueous media was measured (at 27°C) at different pH values, adjusted by the addition of NaOH, to reach pH 6, and HCl, for pH 4 (Figure 9). MOF-5 showed relatively high removal capacities at pH 4 and 6, 750, and 660 mg/g, respectively, but a low value at pH 5 (450 mg/g, without pH adjustment). This behavior may be related to the structure of MOF-5 which has the peculiarity of possessing both acid and basic active sites [52] that may be activated by the change in the pH value (Figure 9).

Table 3: Comparison of maximum adsorption capacity of Pb(II) using different materials.

Adsorbent	Capacity (mg/g)	Reference
Amino-functionalized MNPs	40.10	Hao et al. 2012 [27]
Magnetic nanoadsorbents	36.00	Nassar 2010 [28]
Magnetic nanocomposite beads-chitosan	63.33	Tran et al. 2010 [29]
Hydroxyapatite	1429	Yan et al. 2014 [11]
Biochar-alginate capsule	263.15	Do and Lee 2013 [12]
Chitosan/fe-hydroxyapatite	596.7	Saber-Samandari et al. 2014 [13]
Dry desulfurization slag	130.2	Wu et al. 2014 [9]
MOF-5	658.50	This study

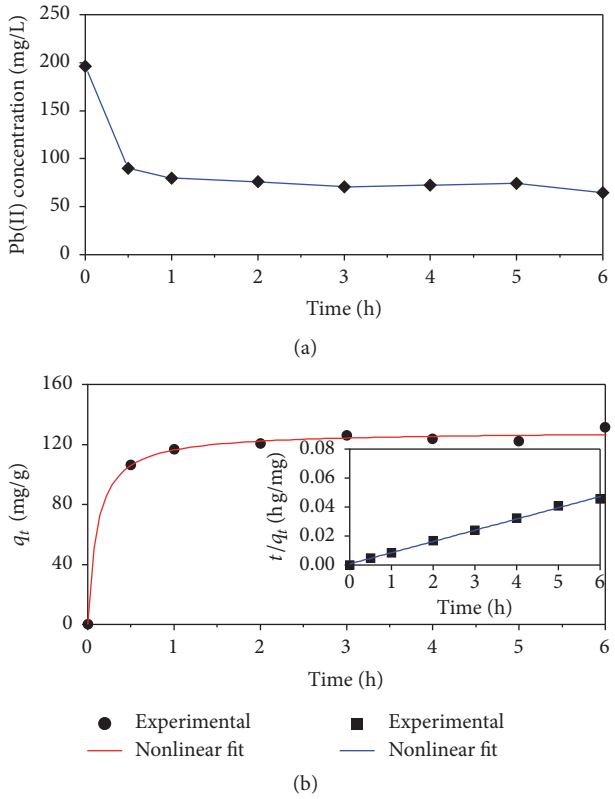

Figure 8: Time evolution of adsorptive removal of Pb(II) (a) and pseudo-second-order kinetics of Pb(II) adsorption onto MOF-5 (b) at 200 mg/L initial Pb(II), 27°C and pH 5.

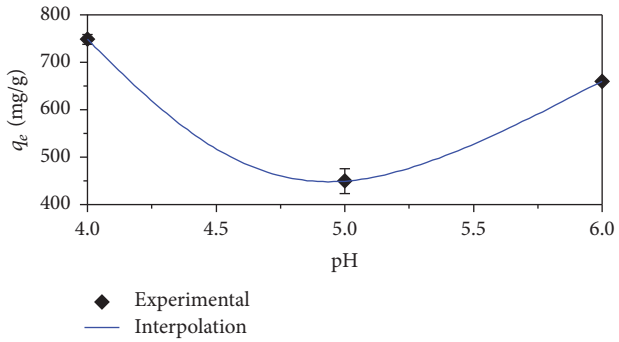

Figure 9: The pH effect on the adsorption of Pb(II) onto MOF-5 using an initial concentration of Pb(II) of 200 mg/L at 27°C.

4. Conclusions

This study demonstrated that MOF-5 performed adequately the adsorption of Pb(II) from aqueous media through a possible process of interaction (BDC^{2-} with Pb(II)) that involved Zn(II) liberation and morphological change of the adsorbent, as shown by SEM-EDX and XPS results. The adsorption of Pb(II) formed a monolayer according to the Langmuir model with a high adsorptive capacity (658.5 mg/g) at pH 5 and 45°C. Furthermore the adsorptive removal capacity of Pb(II) may be improved by changing the pH of the aqueous solution. We may conclude that MOF-5 could be very effective adsorbent material for Pb(II) removal from wastewaters in spite of the loss of the structural stability provoked by the presence of water.

Nomenclature

C_0: Initial concentration of Pb(II) (mg/L)
C_e: Equilibrium concentration of Pb(II) (mg/L)
C_s: Saturation concentration of Pb(II) (mg/L)
h: Initial rate of adsorption (mg/g min)
K_L: Langmuir adsorption constant (L/mg)
K_B: BET adsorption constant (L/mg)
k_2: Rate constant of the pseudo-second-order kinetic model (g/(mg h))
q_e: Equilibrium adsorption capacity (mg/g)
q_{max}: Maximum monolayer adsorption capacity (mg/g)
q_t: Equilibrium adsorption at time t (mg/g)
q_B: Maximum multilayer adsorption capacity (mg/g)
V: Volume of Pb(II) solution (L)
W: Weight of MOF-5 (g).

Competing Interests

The authors declare that there is no conflict of interests regarding the publication of this paper.

Authors' Contributions

José María Rivera and Susana Rincón contributed equally to this work.

Acknowledgments

This research was supported by CONACYT (169563). The authors wish to thank the National Laboratory of Nano and Biomaterials (CONACyT) of the CINVESTAV-Mérida for realizing the SEM-EDX, FTIR, XPS, and XRD analysis, in particular Ph.D. degree holder Patricia Quintana, M.S. degree holder Dora Huerta Quintanilla, Biologist Ana Cristóbal Ramos, and M.S. degree holder Daniel Aguilar Treviño.

References

[1] L. Niu, S. B. Deng, G. Yu, and J. Huang, "Efficient removal of Cu(II), Pb(II), Cr(VI) and As(V) from aqueous solution using an aminated resin prepared by surface-initiated atom transfer radical polymerization," *Chemical Engineering Journal*, vol. 165, no. 3, pp. 751–757, 2010.

[2] A. T. Paulino, L. B. Santos, and J. Nozaki, "Removal of Pb^{2+}, Cu^{2+} and Fe^{3+} from battery manufacture wastewater by chitosan produced from silkworm chrysalides as a low-cost adsorbent," *Reactive and Functional Polymers*, vol. 68, no. 2, pp. 634–642, 2008.

[3] K. N. Dietrich, J. H. Ware, M. Salganik et al., "Effect of chelation therapy on the neuropsychological and behavioral development of lead-exposed children after school entry," *Pediatrics*, vol. 114, no. 1, pp. 19–26, 2004.

[4] K. He, S. Wang, and J. Zhang, "Blood lead levels of children and its trend in China," *Science of the Total Environment*, vol. 407, no. 13, pp. 3986–3993, 2009.

[5] US EPA, "Nutrient criteria tehnical guidance manual: lakes and reservoirs," Document EPA 822-D-99-001, United States Enviromental Protection Agency (USEPA), 1999.

[6] M. E. Argun, S. Dursun, M. Karatas, and M. Gürü, "Activation of pine cone using Fenton oxidation for Cd(II) and Pb(II) removal," *Bioresource Technology*, vol. 99, no. 18, pp. 8691–8698, 2008.

[7] H. Ghassabzadeh, M. Torab-Mostaedi, A. Mohaddespour, M. G. Maragheh, S. J. Ahmadi, and P. Zaheri, "Characterizations of Co (II) and Pb (II) removal process from aqueous solutions using expanded perlite," *Desalination*, vol. 261, no. 1-2, pp. 73–79, 2010.

[8] K. Kadirvelu, K. Thamaraiselvi, and C. Namasivayam, "Removal of heavy metals from industrial wastewaters by adsorption onto activated carbon prepared from an agricultural solid waste," *Bioresource Technology*, vol. 76, no. 1, pp. 63–65, 2001.

[9] Q. Wu, R. You, M. Clark, and Y. Yu, "Pb(II) removal from aqueous solution by a low-cost adsorbent dry desulfurization slag," *Applied Surface Science*, vol. 314, pp. 129–137, 2014.

[10] J.-X. Yu, L.-Y. Wang, R.-A. Chi, Y.-F. Zhang, Z.-G. Xu, and J. Guo, "Competitive adsorption of Pb^{2+} and Cd^{2+} on magnetic modified sugarcane bagasse prepared by two simple steps," *Applied Surface Science*, vol. 268, pp. 163–170, 2013.

[11] Y. Yan, Y. Wang, X. Sun et al., "Optimizing production of hydroxyapatite from alkaline residue for removal of Pb^{2+} from wastewater," *Applied Surface Science*, vol. 317, pp. 946–954, 2014.

[12] X.-H. Do and B.-K. Lee, "Removal of Pb2+ using a biochar-alginate capsule in aqueous solution and capsule regeneration," *Journal of Environmental Management*, vol. 131, pp. 375–382, 2013.

[13] S. Saber-Samandari, S. Saber-Samandari, N. Nezafati, and K. Yahya, "Efficient removal of lead (II) ions and methylene blue from aqueous solution using chitosan/Fe-hydroxyapatite nanocomposite beads," *Journal of Environmental Management*, vol. 146, pp. 481–490, 2014.

[14] K. Ariga, S. Ishihara, H. Abe, M. Li, and J. P. Hill, "Materials nanoarchitectonics for environmental remediation and sensing," *Journal of Materials Chemistry*, vol. 22, no. 6, pp. 2369–2377, 2012.

[15] J.-R. Li, J. Sculley, and H.-C. Zhou, "Metal-organic frameworks for separations," *Chemical Reviews*, vol. 112, no. 2, pp. 869–932, 2012.

[16] A. Vinu and K. Ariga, "New ideas for mesoporous materials," *Advanced Porous Materials*, vol. 1, no. 1, pp. 63–71, 2013.

[17] Z. Chen, S. Xiang, D. Zhao, and B. Chen, "Reversible two-dimensional-three dimensional framework transformation within a prototype metal-organic framework," *Crystal Growth and Design*, vol. 9, no. 12, pp. 5293–5296, 2009.

[18] C. Chen, M. Zhang, Q. Guan, and W. Li, "Kinetic and thermodynamic studies on the adsorption of xylenol orange onto MIL-101(Cr)," *Chemical Engineering Journal*, vol. 183, pp. 60–67, 2012.

[19] E. Haque, J. E. Lee, I. T. Jang et al., "Adsorptive removal of methyl orange from aqueous solution with metal-organic frameworks, porous chromium-benzenedicarboxylates," *Journal of Hazardous Materials*, vol. 181, no. 1–3, pp. 535–542, 2010.

[20] Z. Hasan, J. Jeon, and S. H. Jhung, "Adsorptive removal of naproxen and clofibric acid from water using metal-organic frameworks," *Journal of Hazardous Materials*, vol. 209-210, pp. 151–157, 2012.

[21] Z. Hasan and S. H. Jhung, "Removal of hazardous organics from water using metal-organic frameworks (MOFs): plausible mechanisms for selective adsorptions," *Journal of Hazardous Materials*, vol. 283, pp. 329–339, 2015.

[22] F. Ke, L.-G. Qiu, Y.-P. Yuan et al., "Thiol-functionalization of metal-organic framework by a facile coordination-based postsynthetic strategy and enhanced removal of Hg^{2+} from water," *Journal of Hazardous Materials*, vol. 196, pp. 36–43, 2011.

[23] M. Maes, S. Schouteden, L. Alaerts, D. Depla, and D. E. De Vos, "Extracting organic contaminants from water using the metal-organic framework $Cr^{III}(OH)\cdot O_2C–C_6H_4–CO_2$," *Physical Chemistry Chemical Physics*, vol. 13, no. 13, pp. 5587–5589, 2011.

[24] K. Yang, Q. Sun, F. Xue, and D. Lin, "Adsorption of volatile organic compounds by metal-organic frameworks MIL-101: influence of molecular size and shape," *Journal of Hazardous Materials*, vol. 195, pp. 124–131, 2011.

[25] N. Bakhtiari and S. Azizian, "Adsorption of copper ion from aqueous solution by nanoporous MOF-5: a kinetic and equilibrium study," *Journal of Molecular Liquids*, vol. 206, pp. 114–118, 2015.

[26] N. A. Rodríguez, R. Parra, and M. A. Grela, "Structural characterization, optical properties and photocatalytic activity of MOF-5 and its hydrolysis products: implications on their excitation mechanism," *RSC Advances*, vol. 5, no. 89, pp. 73112–73118, 2015.

[27] S. Y. Hao, Y. J. Zhong, F. Pepe, and W. Zhu, "Adsorption of Pb^{2+} and Cu^{2+} on anionic surfactant-templated amino-functionalized mesoporous silicas," *Chemical Engineering Journal*, vol. 189-190, pp. 160–167, 2012.

[28] N. N. Nassar, "Rapid removal and recovery of Pb(II) from wastewater by magnetic nanoadsorbents," *Journal of Hazardous Materials*, vol. 184, no. 1–3, pp. 538–546, 2010.

[29] H. V. Tran, L. D. Tran, and T. N. Nguyen, "Preparation of chitosan/magnetite composite beads and their application for

removal of Pb(II) and Ni(II) from aqueous solution," *Materials Science and Engineering C*, vol. 30, no. 2, pp. 304–310, 2010.

[30] J. Hafizovic, M. Bjørgen, U. Olsbye et al., "The inconsistency in adsorption properties and powder XRD data of MOF-5 is rationalized by framework interpenetration and the presence of organic and inorganic species in the nanocavities," *Journal of the American Chemical Society*, vol. 129, no. 12, pp. 3612–3620, 2007.

[31] J. A. Greathouse and M. D. Allendorf, "The interaction of water with MOF-5 simulated by molecular dynamics," *Journal of the American Chemical Society*, vol. 128, no. 33, pp. 10678–10679, 2006.

[32] M. Eddaoudi, H. Li, and O. M. Yaghi, "Highly porous and stable metal-organic frameworks: structure design and sorption properties," *Journal of the American Chemical Society*, vol. 122, no. 7, pp. 1391–1397, 2000.

[33] S. L. James, "Metal-organic frameworks," *Chemical Society Reviews*, vol. 32, no. 5, pp. 276–288, 2003.

[34] S. Keskin and S. Kizilel, "Biomedical applications of metal organic frameworks," *Industrial and Engineering Chemistry Research*, vol. 50, no. 4, pp. 1799–1812, 2011.

[35] S. Keskin and D. S. Sholl, "Efficient methods for screening of metal organic framework membranes for gas separations using atomically detailed models," *Langmuir*, vol. 25, no. 19, pp. 11786–11795, 2009.

[36] A. V. Neimark, F.-X. Coudert, C. Triguero et al., "Structural transitions in MIL-53 (Cr): view from outside and inside," *Langmuir*, vol. 27, no. 8, pp. 4734–4741, 2011.

[37] S. Das, H. Kim, and O. Kim, "Metathesis in single crystal: complete and reversible exchange of metal ions constituting the frameworks of metal-organic frameworks," *Journal of the American Chemical Society*, vol. 131, no. 11, pp. 3814–3815, 2009.

[38] N. Iswarya, M. G. Kumar, K. S. Rajan, and R. J. B. Balaguru, "Synthesis, characterization and adsorption capability of MOF-5," *Asian Journal of Scientific Research*, vol. 5, no. 4, pp. 247–254, 2012.

[39] R. Sabouni, H. Kazemian, and S. Rohani, "A novel combined manufacturing technique for rapid production of IRMOF-1 using ultrasound and microwave energies," *Chemical Engineering Journal*, vol. 165, no. 3, pp. 966–973, 2010.

[40] J. E. Huheey, E. A. Keiter, A. Ellen et al., *Inorganic Chemistry: Principles of Structure and Reactivity*, Harper Collings College Publishers, 4th edition, 1993.

[41] J. Coates, "Interpretation of infrared spectra: a practical approach," in *Encyclopedia of Analytical Chemistry*, R. A. Meyers, Ed., pp. 10815–10837, John Wiley & Sons, New York, NY, USA, 2000.

[42] N. T. S. Phan, K. K. A. Le, and T. D. Phan, "MOF-5 as an efficient heterogeneous catalyst for Friedel-Crafts alkylation reactions," *Applied Catalysis A: General*, vol. 382, no. 2, pp. 246–253, 2010.

[43] B. R. Strohmeier, "Zinc aluminate ($ZnAl_2O_4$) by XPS," *Surface Science Spectra*, vol. 3, no. 2, pp. 128–134, 1994.

[44] L. Y. Wu, H. J. Wang, H. C. Lan, H. Liu, and J. Qu, "Adsorption of Cu(II)–EDTA chelates on tri-ammonium-functionalized mesoporous silica from aqueous solution," *Separation and Purification Technology*, vol. 117, pp. 118–123, 2013.

[45] J. Chastain and J. F. Moulder, *Handbook of X-ray Photoelectron Spectroscopy: A Reference Book of Standard Spectra for Identification and Interpretation of XPS Data*, Perkin-Elmer, Eden Prairie, Minn, USA, 1992.

[46] H. S. Liu, T. S. Chin, and S. W. Yung, "FTIR and XPS studies of low-melting PbO–ZnO–P_2O_5 glasses," *Materials Chemistry and Physics*, vol. 50, no. 1, pp. 1–10, 1997.

[47] I. Langmuir, "The constitution and fundamental properties of solids and liquids. Part I. Solids," *Journal of the American Chemical Society*, vol. 38, no. 2, pp. 2221–2295, 1916.

[48] B. H. Hameed and A. A. Rahman, "Removal of phenol from aqueous solutions by adsorption onto activated carbon prepared from biomass material," *Journal of Hazardous Materials*, vol. 160, no. 2-3, pp. 576–581, 2008.

[49] K. Y. Foo and B. H. Hameed, "Insights into the modeling of adsorption isotherm systems," *Chemical Engineering Journal*, vol. 156, no. 1, pp. 2–10, 2010.

[50] R. Rostamian, M. Najafi, and A. A. Rafati, "Synthesis and characterization of thiol-functionalized silica nano hollow sphere as a novel adsorbent for removal of poisonous heavy metal ions from water: kinetics, isotherms and error analysis," *Chemical Engineering Journal*, vol. 171, no. 3, pp. 1004–1011, 2011.

[51] T. Sheela and Y. A. Nayaka, "Kinetics and thermodynamics of cadmium and lead ions adsorption on NiO nanoparticles," *Chemical Engineering Journal*, vol. 191, pp. 123–131, 2012.

[52] L. Wang, B. Xiao, G. Y. Wang, and J. Wu, "Synthesis of polycarbonate diol catalyzed by metal-organic framework $Zn_4O[CO_2\text{-}C_6H_4\text{-}CO_2]_3$," *Science China Chemistry*, vol. 54, no. 9, pp. 1468–1473, 2011.